

## Supplementary File

### Raman Spectroscopy of Carbonaceous Material

Four samples of Orocopia Schist from Cemetery Ridge and three samples of Orocopia Schist from the Plomosa Mountains were analyzed by Raman Spectroscopy of Carbonaceous Material (RSCM) to determine maximum (peak) burial/metamorphic temperatures. Carbonaceous material was analyzed on uncovered thin-section for each sample at the University of Wyoming on a Renishaw inVia Reflex confocal Raman spectrometer. Measurements were made with a 532 nm laser operated at a power of 3-5 mW (measured at the sample interface) and was focused using a 20x objective. The probed area for each measurement is  $\sim 1\mu$  in diameter. Carbonaceous material was analyzed for 90 seconds over a spectral window of  $1200\text{-}1900\text{ cm}^{-1}$ . Thin-sections were cut normal to bedding the laser was focused on carbonaceous material located beneath transparent minerals (usually quartz), following the procedures and recommendations of Beyssac et al. (2003). Thirty to forty analyses were made on each thin section. Outliers were removed using the Thompson Tau statistical method. Reported temperatures are unweighted averages for each thin-section and uncertainty (in  $^{\circ}\text{C}$ ) is reported at the  $2\sigma$  level using the standard deviation of each set of measurements and uncertainty from the calibration equation of Rahl et al. (2005) added in quadrature. The equations of Rahl et al. (2005) were used to convert the height ratio (R1) and area ratio (R2) of first-order Raman peaks (G, D1, and D2) into temperatures. The method is valid for temperatures in the range of  $100\text{-}700\text{ }^{\circ}\text{C}$ . Peak positions, heights, widths, and area for Raman Spectra were calculated using a modified version of a peak-fitting program written by E. Soignard (Long and Soignard, 2016) that allows peaks to be fit mathematically (i.e., not by hand) using a combination of Gaussian and Lorentzian peaks. Raw data collected for each sample is presented in a table at the end of this document.

**TABLE S1:** Summary of Raman Spectroscopy of Carbonaceous Material Results

Sample	Location	Lat	Long	Avg. Temp. ( $^{\circ}\text{C}$ )	Unc. ( $2\sigma$ )
CEM-5	Cemetery Ridge	33.38031	-113.48427	633	38
CEM-J	Cemetery Ridge	33.38447	-113.48887	599	47
CEM-10	Cemetery Ridge	33.37746	-113.48251	649	29
OS19pel	Cemetery Ridge	33.38443	-113.48757	602	37
PLM-3	Plomosa Mtns.	33.92638	-114.08480	583	38
PLM-4	Plomosa Mtns.	33.93470	-114.08697	546	34
PLM-6	Plomosa Mtns.	33.91934	-114.08445	573	44

### Details of Numerical Modeling

The models are two-dimensional and the model domain is 400 km wide by 70 km deep. The models are intended to represent a trench-perpendicular cross-section of a low-angle subduction zone where the trench would be located to the left of the model. The continental crust is represented by a 30 km deep rectangle. The Orocopia Schist is represented by a 10 km thick body located at 50-60 km depth on the left side (trench) of the model and at 60-70 km on the right

side (landward) of the model. This geometry is intended to represent sediments being subducted at a low angle ( $\sim 1.4^\circ$  dip). The polygon located between the “Orocopia Schist” and “continental crust” represented continental mantle lithosphere.

The equations for heat transport, motion, and continuity (momentum, mass, and energy) are solved for plane strain and laminar flow of incompressible, Newtonian (“mantle lithosphere”) and non-Newtonian (“continental crust” and “Orocopia Schist”) fluids using COMSOL Multiphysics 5.4, a finite-element software package that has been used and benchmarked for subduction zone processes (e.g., van Keken et al., 2008). The resolution is uniform and is physics controlled, but generally represented by a triangular mesh with side lengths of 2-5 km. Experimental runs of the model with higher resolution did not affect the model results. The time-step for all models was 1 Myr.

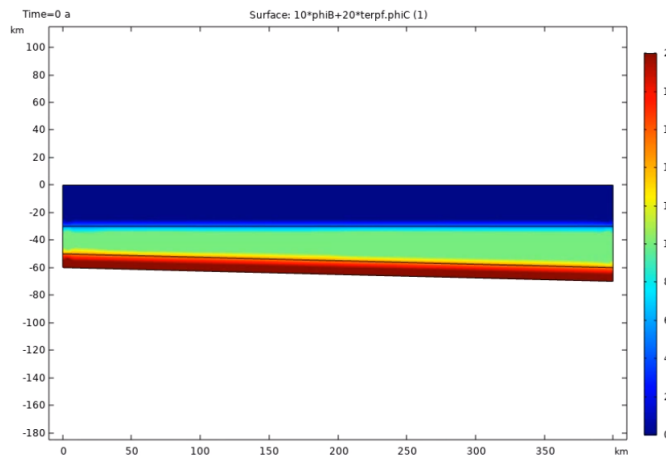


Figure S1: Geometry of the reference model. The 3 domain materials are modeled as phases (fluids) shown above using a dimensionless scale where 20 = Orocopia Schist, 10 = continental mantle lithosphere, and 0 = continental crust.

temperature at the base of the model (873 °K in reference model). In addition, the left boundary of Model 2, above the inlet, was held at a constant temperature gradient (i.e., not thermally insulated) that matched the initial thermal gradient in the rest of the model. This helped to prevent anomalous heating of the model boundary related to the (constant temperature) inlet. The model was run using the Three-Phase Flow, Phase field interface option, which accounts for surface tension between three immiscible phases (fluids), the contact angles with the walls, and the density and viscosity of each fluid. The phase field variables are measures of the content of each phase in every point in space. The three phases modeled are “continental crust,” “continental mantle lithosphere,” and “Orocopia Schist.”

Material properties varied between each of the domains in the reference model. In the “continental crust” domain, density varied linearly with depth, increasing from 2600 kg/m<sup>3</sup> at the surface to 2900 kg/m<sup>3</sup> at 30 km depth. Dynamic viscosity was calculated using the wet quartz flow law of Hirth et al. (2001). Viscosity was calculated at each time step using the temperatures

The top and sides of the model are no-slip boundaries. All interior domain boundaries and the bottom of the model are free-slip boundaries. The top of the model (representing the crust-air interface) was fixed and not deformable. Model 2 includes a 10-km tall inlet at the bottom left of the model where “Orocopia Schist” material is added to the model at a rate of 10 cm/yr. Gravity was constant at 9.81 m/s<sup>2</sup> throughout all models. The sides of the model were thermally insulated and the top and bottom were held at a constant temperature, 273 °K and 873 °K respectively. for the reference model, but varied as part of model trial runs. In Model 2, the temperature of the added Orocopia Schist was held constant and equaled the

returned from the model, a quartz material parameter ( $A_q$ ) of  $1.36742 \times 10^{-5}$  MPa<sup>-n</sup>/s with a stress exponent ( $n_q$ ) of 4, a quartz activation energy ( $Q$ ) of 135 kJ/mol, water fugacity ( $f_{\text{H}_2\text{O}}$ ) of 1,000 MPa, and a strain rate of  $10^{-15}$  s<sup>-1</sup>. Strain rates as high  $10^{-13}$  s<sup>-1</sup> have been estimated for the Pelona Schist based on deformed quartz fabrics (Xia and Platt, 2017), although this is likely not applicable to the Orocopia Schist as a whole. The strain applied in the modeling in this study ( $10^{-15}$  s<sup>-1</sup>) is based on estimates of the strain rates experienced by the continental mantle lithosphere near the slab interface in the region of flat-slab subduction in the numerical modeling studies of Axen et al. (2018) and Liu and Currie (2019). Viscosity was updated after each time step based on temperature, although strain rate was held constant.

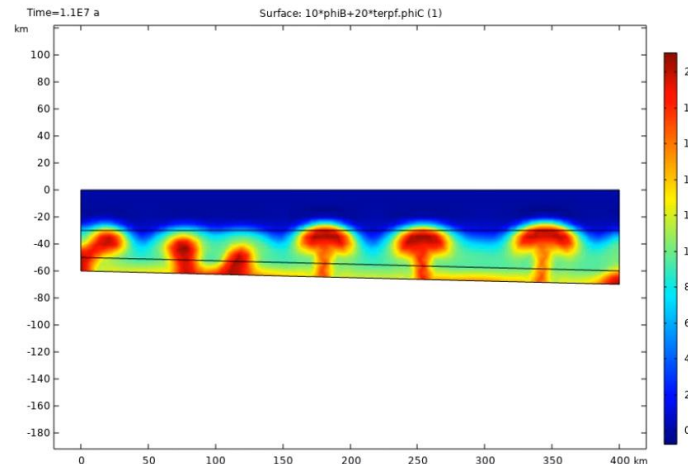


Figure S2: A single time step in one of the model trial runs exploring variable viscosities.

These parameters resulted in effective viscosities of  $>10^{23}$  Pa·s in the upper crust and  $\sim 10^{21}$  Pa·s at the base of the crust. Variations in viscosity were explored by changing the temperature or strain rate. The continental mantle lithosphere domain was modeled using a constant density of 3350 kg/m<sup>3</sup> and a constant dynamic viscosity of  $10^{21}$  Pa·s. Variable viscosity was explored as part of the model trial runs. The Orocopia Schist domain was modeled with a constant density of 2800 kg/m<sup>3</sup> and a dynamic viscosity based on the wet quartzite flow law using the same parameters as described for the crust domain above. These parameters resulted in an initial effective viscosity of  $>\sim 10^{20}$  Pa·s for the Orocopia Schist at the start of the model run. For all three domains, heat capacity was set at 1000 J/(kg·K), the ratio of specific heats ( $\gamma$ ) was set at 1, and thermal conductivity was set at 2.5 W/(m·K).

## REFERENCES CITED

- Axen, G.J., van Wijk, J.W. and Currie, C.A., 2018, Basal continental mantle lithosphere displaced by flat-slab subduction: *Nature Geoscience*, v. 11, p. 961–964.
- Beyssac, O., Goffe, B., Petitet, J.P., Froigneux, E., Moreau, M., and Rouzaud, J.N., 2003, On the characterization of disordered and heterogeneous carbonaceous materials by Raman spectroscopy: *Spectrochimica Acta Part A*, v. 59, p. 2267–2276.
- Hirth, G., Teyssier, C., and Dunlap, J.W., 2001, An evaluation of quartzite flow laws based on comparisons between experimentally and naturally deformed rocks: *International Journal of Earth Sciences*, v. 90, p. 77–87.
- Liu, X. and Currie, C.A., 2019, Influence of Upper Plate Structure on Flat-slab Depth: Numerical modeling of subduction dynamics: *Journal of Geophysical Research: Solid Earth*, v. 124, p. 13150–13167.

- Long, S.P. and Soignard, E., 2016, Shallow-crustal metamorphism during Late Cretaceous anatexis in the Sevier hinterland plateau: Peak temperature conditions from the Grant Range, eastern Nevada, USA: *Lithosphere*, v. 8, p. 150-164.
- Rahl, J.M., Anderson, K.M., Brandon, M.T., and Fassoulas, C., 2005, Raman spectroscopic carbonaceous material thermometry of low-grade metamorphic rocks: Calibration and application to tectonic exhumation in Crete, Greece: *Earth and Planetary Science Letters*, v. 240, p. 339–354.
- van Keken, P.E., Currie, C., King, S.D., Behn, M.D., Cagnioncle, A., He, J., Katz, R.F., Lin, S.C., Parmentier, E.M., Spiegelman, M., and Wang, K., 2008, A community benchmark for subduction zone modeling: *Physics of the Earth and Planetary Interiors*, v. 171, p. 187-197.
- Xia, H. and Platt, J.P., 2017, Structural and rheological evolution of the Laramide subduction channel in southern California: *Solid Earth*, v. 8, p. 379-403.

Table S2: Raman Spectroscopy data

Analysis	D1_width	D1_area	D1_height	D1_position	D2_width	D2_area	D2_height	D2_position	G_width	G_area	G_height	G_position	R1_calc	R2_calc
PLM-6-3	30	1602	34	1357					17	14233	533	1583		0.06378987 0.1011683
PLM-6-5	48	17945	238	1350	10	1553	146	1625	17	57706	2161	1581		0.1101342 0.23243614
PLM-6-7	79	22585	182	1352	120	5488	43	1670	15	146555	6220	1581		0.02926045 0.12933207
PLM-6-13	39	8332	136	1355	9	718	75	1623	17	77520	2903	1581		0.04684809 0.09624581
PLM-6-15	65	15009	147	1353	10	989	93	1623	17	72019	2697	1581		0.05450501 0.17052388
PLM-6-17	41	10047	156	1354	16	1327	78	1621	19	32173	1078	1581		0.14471243 0.23071624
PLM-6-18	59	11955	129	1348	9	1053	110	1623	17	83529	3128	1581		0.04124041 0.12383853
PLM-6-19	43	8848	131	1351	19	2101	104	1624	19	33904	1136	1580		0.1153169 0.19726663
PLM-6-20	43	12428	184	1355	11	1848	158	1624	17	47292	1771	1582		0.1038961 0.20185811
PLM-6-21	38	16594	278	1355	9	1216	127	1622	17	53140	1990	1582		0.13969849 0.23388302
PLM-6-23	38	9431	158	1356	10	915	86	1626	18	40941	1448	1582		0.10911602 0.18388675
PLM-6-24	3	9106	187	1358	10	1021	96	1624	17	35489	1329	1582		0.1407073 0.19962294
PLM-6-25	40	11938	190	1355	9	861	90	1624	17	35809	1341	1582		0.14168531 0.24559743
PLM-6-26	32	5881	117	1356	10	842	72	1624	17	19974	748	1583		0.15641711 0.22028692
PLM-6-27	62	17043	175	1343	15	957	60	1622	17	50657	1897	1581		0.09225092 0.24823397
PLM-6-28	46	13367	185	1356	13	1383	100	1624	18	51261	1813	1582		0.10204082 0.20249655
PLM-6-29	53	7909	95	1351	10	404	38	1622	18	58132	2056	1581		0.04620623 0.11903078
PLM-6-30	38	7282	122	1356	11	702	60	1624	17	35996	1348	1582		0.09050445 0.16557526
PLM-6-31	55	5702	66	1353	9	306	32	1624	17	40349	1511	1582		0.04367968 0.12300192
PLM-6-32	52	9720	119	1355	9	938	98	1624	17	62243	2331	1581		0.05105105 0.1333315
PLM-6-33	60	85860	911	1338	32	27021	794	1615	17	306423	11475	1578		0.07938998 0.2047679
PLM-6-34	46	73350	1022	1352	11	9563	833	1620	17	256814	9502	1580		0.1075563 0.21590866
PLM-4-1	45	91892	1300	1347	13	27097	1960	1619	18	337200	11926	1579		0.10900553 0.20143405
PLM-4-2	55	86394	1000	1350	15	14357	900	1621	18	424115	15000	1581		0.06666667 0.16460201
PLM-4-3	36	104785	1853	1354	8	7113	836	1622	17	567423	21249	1579		0.0872041 0.15424961
PLM-4-4	47	87043	1179	1353	12	16424	1287	1620	17	234964	8799	1580		0.1339925 0.25719571
PLM-4-6	39	184580	3013	1353	8	15152	1781	1622	16	606001	24112	1580		0.12495853 0.22908333
PLM-4-7	50	111527	1420	1355	7	5189	691	1622	15	667840	28344	1580		0.05009879 0.14215301
PLM-4-10	39	118111	1928	1353	14	19459	1307	1622	16	361560	14386	1580		0.13401919 0.23663374
PLM-4-11	38	152330	2552	1353	9	11878	1241	1622	16	545908	21721	1580		0.11748999 0.21451425
PLM-4-12	49	118147	1535	1349	16	36703	2157	1618	16	496899	19771	1579		0.07763897 0.18127684
PLM-4-13	41	187283	2908	1353	16	26697	1569	1620	17	482720	18077	1580		0.1608674 0.26881441
PLM-4-15	32	120838	2404	1353	11	15219	1301	1621	16	341579	13591	1580		0.17688176 0.25299182
PLM-4-16	33	156338	3016	1354	11	17313	1480	1620	15	502034	21307	1579		0.14154973 0.23137705
PLM-4-17	37	154017	2650	1352	13	19673	1423	1620	16	371789	14793	1579		0.17913878 0.28235184
PLM-4-18	44	224624	3250	1349	12	21912	1717	1619	17	720996	27000	1579		0.12037037 0.23216183
PLM-4-20	42	117631	1783	1352	12	12481	978	1620	16	551362	21938	1580		0.0812745 0.1726126
PLM-4-21	37	107463	1849	1352	14	16214	1089	1621	16	389005	15478	1580		0.11945988 0.20960947
PLM-4-23	42	102325	1551	1354	10	11103	1044	1622	16	405391	16130	1580		0.09615623 0.19722678
PLM-4-24	47	94351	1278	1352	12	12379	970	1621	17	419539	15711	1580		0.08134428 0.17928284
PLM-4-25	51	169033	2110	1352	12	14063	1102	1621	16	579159	23044	1580		0.09156396 0.22175388
PLM-3-1	50	64795	825	1353	17	17410	963	1619	18	273893	9687	1580		0.08516569 0.18195834
PLM-3-2	38	115799	1940	1355	8	13595	1598	1622	18	415265	14687	1581		0.1320896 0.21260826
PLM-3-4	50	58905	750	1351	15	15984	1002	1619	18	371440	13137	1581		0.05709066 0.13197664
PLM-3-6	43	61263	907	1353	10	7423	698	1623	17	390913	14639	1581		0.06195778 0.13329663
PLM-3-7	40	94876	1510	1354	8	11145	1310	1622	17	332860	12465	1580		0.12113919 0.21617705
PLM-3-8	38	51334	860	1355	14	11092	745	1621	16	355075	14128	1580		0.06087203 0.12295539
PLM-3-10	43	70854	1049	1354	10	15410	1449	1621	17	299213	11205	1580		0.09361892 0.18380863
PLM-3-11	54	97886	1154	1350	8	5870	690	1622	17	557837	20890	1579		0.05524174 0.14795501
PLM-3-12	63	66501	672	1351	7	5062	680	1622	17	403464				

OS19pel-20	47	52491	711	1348					16	369552	14704	1580		0.04835419	0.12437358
OS19pel-21	32	67708	1347	1352	8	7078	832	1621	16	260250	10355	1580		0.13008209	0.20209172
OS19pel-23	39	107636	1757	1353	9	10146	1060	1621	15	392966	16678	1579		0.10534836	0.21074189
CEM10-3	70	121391	1104	1350	21	14606	654	1614	17	407843	15273	1579		0.07228442	0.22321087
CEM10-6	43	52009	770	1352	11	4328	370	1621	19	449378	15057	1580		0.05113901	0.10284251
CEM10-8	50	42097	536	1351	1	38	36	1621	17	649644	24328	1579		0.02203223	0.06085325
CEM10-10	35	107097	1948	1354	7	7571	1017	1622	17	625984	23442	1580		0.08309871	0.14459827
CEM10-11	48	97565	1294	1352	8	4960	583	1622	18	630037	22283	1580		0.05807118	0.13318327
CEM10-14	108	46822	276	1350	5	1430	269	1620	16	517961	20609	1579		0.01339221	0.08269326
CEM10-15	98	191807	1246	1353	14	4169	280	1619	15	619891	26309	1580		0.04736022	0.23509592
CEM10-16	50	119852	1526	1354	16	14855	873	1619	16	605724	24101	1579		0.06331687	0.16186789
CEM10-19	36	33138	586	1354	7	2300	309	1621	15	677783	28766	1579		0.02037127	0.04646246
CEM10-20	41	124104	1927	1354	7	8152	1095	1622	17	359643	13468	1580		0.14307989	0.25229569
CEM10-22	34	48600	910	1350	6	4090	641	1622	15	512779	21763	1581		0.04181409	0.08594636
CEM10-23	42	66435	1007	1354	10	2999	282	1621	19	507725	17012	1580		0.05919351	0.11510693
CEM10-24	68	62700	587	1348	6	2291	359	1623	15	545695	23160	1580		0.02534542	0.10267142
CEM10-25	36	87764	1552	1355	7	2836	381	1622	15	317379	13470	1580		0.11521901	0.21511892
CEM10-26	36	48406	856	1354	6	3554	557	1622	15	501375	21279	1580		0.04022745	0.08748046
CEM10-27	33	52303	1009	1353	6	6802	1066	1622	16	577425	22975	1580		0.0439173	0.08216895
CEM10-28	35	70215	1140	1348	7	5436	537	1620	17	618345	23303	1580		0.04892074	0.10117493
CEM10-29	40	29719	473	1353	2	791	372	1622	15	484622	20568	1581		0.02299689	0.05769201
CEM10-30	44	85495	1237	1351	10	7317	688	1620	16	575791	22910	1580		0.05399389	0.1278711
CEMJ-1	43	89564	1326	1353	7	2896	389	1621	19	773556	25919	1579		0.05115938	0.10342072
CEMJ-2	55	63586	736	13540	9	1292	135	1622	16	706632	28116	1579		0.02617727	0.0824176
CEMJ-4	150	76341	324	1350	50	2659	50	1620	16	597506	23774	1580		0.01362833	0.11284601
CEMJ-5	45	173110	2449	1352	12	9303	729	1621	19	654384	21926	1580		0.11169388	0.20687216
CEMJ-7	39	77005	1257	1353	8	5989	704	1622	16	567095	22564	1580		0.05570821	0.11845301
CEMJ-8	50	129591	1650	1353	37	35728	908	1623	17	544191	20379	1580		0.0809657	0.18264859
CEMJ-9	50	62832	800	1350	13	8378	606	1620	17	344849	12914	1580		0.06194827	0.15101704
CEMJ-10	42	89196	1352	1352	11	4785	409	1621	20	444504	14149	1580		0.09555446	0.1656425
CEMJ-11	50	147655	1880	1348	31	14407	437	1616	20	489649	15586	1580		0.12062107	0.22656515
CEMJ-13	35	119632	2176	1355	8	6236	733	1622	17	562697	21072	1580		0.103265	0.17374104
CEMJ-14	33	59508	1148	1353	5	851	160	1622	19	936809	31389	1580		0.03657332	0.05967701
CEMJ-15	28	147956	3364	1352	8	7529	885	1621	21	923628	28000	1580		0.12014286	0.1371089
CEMJ-16	61	184355	1924	1350	20	14889	700	1620	22	742987	21500	1580		0.08948837	0.19565796
CEMJ-17	40	186108	2962	1353	9	12634	1320	1621	18	812774	28746	1579		0.10304042	0.18398918
CEMJ-19	54	149967	1768	1350	9	7312	764	1621	17	506299	18960	1580		0.09324895	0.22599755
CEMJ-20	50	44611	568	1353	4	417	98	1624	19	420786	14099	1580		0.04028655	0.09576999
CEMJ-21	42	62873	953	1353	14	6491	436	1620	17	339375	12709	1580		0.07498623	0.15382188
CEM5-1a	50	78540	1000	1350	14	14591	980	1621	15	365752	15523	1580		0.06442054	0.17115474
CEM5-1b	26	70695	1731	1359	9	14070	1470	1622	15	345277	14654	1581		0.11812474	0.16439092
CEM5-5	38	68499	1140	1353	10	10211	940	1622	16	373736	14426	1581		0.07902398	0.15139707
CEM5-6	32	71377	1420	1354	6	4352	682	1622	17	699873	26209	1580		0.05417986	0.09202787
CEM5-7	40	33552	534	1352	6	2221	348	1622	17	564513	21140	1580		0.02526017	0.05589336
CEM5-8	49	37484	487	1353	28	11613	390	1617	16	204279	8128	1581		0.05991634	0.14793824
CEM5-10	37	104810	1820	1355	4	1876	402	1623	15	504957	21461	1580		0.084805	0.17135813
CEM5-11	33	89314	1723	1353	9	9275	969	1621	18	651299	23035	1581		0.07479922	0.11910312
CEM5-12	50	54664	696	1350	13	6940	502	1619	15	322280	13678	1581			